

Implementation of Speed and Torque Control on Quadrotor Altitude and Attitude Stability

Elmer R. Magsino*, Christian Michael Dollosa, Samuel Gavinio, Gerard Hermoso, Nico Laco, and Louise Angelo Roberto

Electronics and Communications Department, De La Salle University, 2401 Taft Avenue, Manila, Philippines

*E-mail: elmer.magsino@dlsu.edu.ph

Most quadrotor flight controllers make use of an attitude control loop, which is responsible for stabilizing the flight of the vehicle by directly driving the four motors via the electronic speed controllers (ESCs). Such a control loop loses its effectiveness when the motors and ESCs are not well matched resulting in variation of the control performance. This study presents an alternative control structure that incorporates an inner speed and torque control loop within the attitude and altitude loop in order to achieve better flight stability and maneuverability. The control structure is designed to make use of PID control in order to correct for errors in the process and drive the motors correspondingly. The control system is simulated and tuned using Simulink and later implemented on a dsPIC33 microcontroller where various feedback and instrumentation sensors are interfaced. The attitude feedback is implemented using a complementary filter to fuse the accelerometer and gyrometer data in order to arrive at usable attitude estimates. The result of the flight testing reveals that the experimental and simulation results vary only by an attitude standard deviation of less than 5° and an altitude standard deviation of 50 cm. The control structure not only compensates for motor and ESC mismatches but also allows the attitude control loop, the one whose effects on the stability is most visible, to operate at the range of operation.

1. INTRODUCTION

A quadrotor, shown in Figure 1, is one of the widely known subsets of vertical-takeoff-and landing-type aircraft, and it consists of four rotors with two pairs rotating in the opposite direction of each other (Corke, 2011). The identifying characteristic of such an aircraft is the amount of stability that can be obtained from using four separate propulsion motors to precisely control the vehicle's movement and flight. Figure 1 demonstrates the quadrotor in a "+" notation showing the four rotors, their thrust vectors, and

directions of rotation. The body-fixed frame {B} is attached to the vehicle and has its origin at the vehicle's center of mass. Rotors 1 and 3 rotate counterclockwise (viewed from above) while rotors 2 and 4 rotate clockwise. The relationship between the rotor speed, ω_i , and the upward thrust (in the vehicle's negative z direction) is given by Equation 1:

$$T_i = b\omega_i^2, i = 1,2,3,4 \quad (1)$$

where $b > 0$ is the lift constant that depends on the air density, the cube of the rotor blade radius, the

number of blades, and the chord length of the blade (Corke, 2011). The simplified derivation of the different states needed in making a quadrotor achieve a stable flight is also shown in Corke (2011).

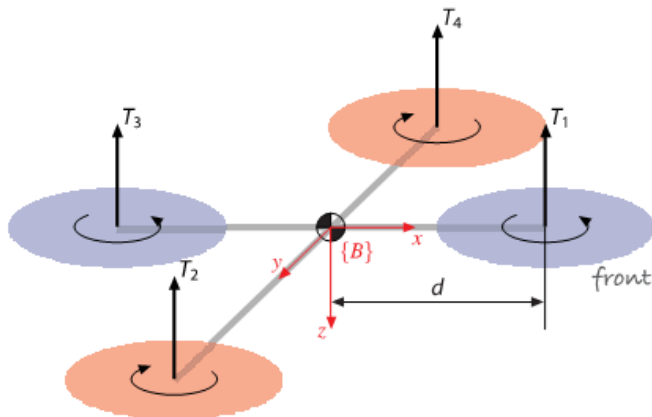


Figure 1. Quadrotor Model

Quadrotor helicopters have become increasingly popular as a field of research due to their several unique characteristics versus a typical two-rotor helicopter. In addition to the capability of achieving great flight control, they are preferred over a typical helicopter because they do not possess complicated linkages and joints, which, in turn, simplify the necessary mechanical setup (Hoffman et al., 2007). The design and implementation of quadrotors have recently become an extensively researched field in many areas such as in the military and robotics as emphasized in papers like “Modelling, Identification and Control of a Quadrotor Helicopter” (Bresciani, 2008) and “Design and Control of a Quad-Rotor Flying Robot for Aerial Surveillance” (Weng, 2006).

One of the research fields when it comes to implementing such quadrotor platforms is the implementation of the control system because of its direct significance on the actual flight capability of the vehicle. Various control systems, in order to attain stability during the performance of various flight maneuvers, have been employed in different studies. However, the implementation of a closed-loop control system having feedback from the speed and torque for each individual motor in order

to achieve better control has been very rarely accomplished.

This research focuses on achieving attitude and altitude flight stability through component modeling and control. In short, controlling the motors properly allows the stable vertical-takeoff-and-landing flight of a quadrotor. Theoretically, if equal thrust is exerted by each motor, then vertical flight stability is achieved.

Having stated this, the primary focus of this study is the development of a closed-loop speed and torque control system that can be implemented for a particular quadrotor platform. The control loop implemented in this study involves an inner torque loop (dashed box) and an outer speed loop. This torque–speed loop structure is illustrated in Figure 2.

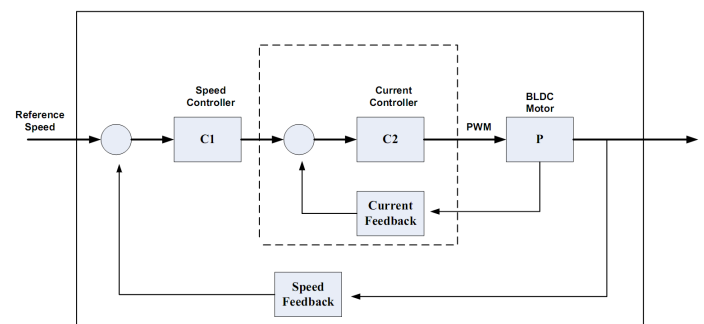


Figure 2. Torque–Speed Control Structure for Each BLDC Motor

The outer loop speed controller monitors the rotor speed through voltage measurements and establishes the set value for the inner current controller based on the desired speed and the actual output speed of the motor. The internal torque loop, in turn, is responsible for providing the necessary pulse-width-modulated (PWM) signal to the controller of the brushless DC (BLDC) motor by sampling the motor current at a much faster rate than the speed controller. Each BLDC motor is to be controlled using its own control loop, allowing for the ability to independently control each of the four motors.

The choice of current as the inner parameter to be regulated as opposed to speed is because the current drawn by a motor, which is a direct

resultant of the torque, is more prone to changes as opposed to the rotor speed.

Both speed and current controllers are to be implemented using the PID control technique. The influence of the use of PID control in the stability of a flight of a quadrotor is one of the main focuses of many quadrotor studies that are being conducted.

The study by Li and Li (2011) discusses the analysis of a quadrotor's characteristics implemented with PID control. Their quadrotor platform is constructed out of carbon fiber and was tested in obstacle-free areas with little wind disturbance.

The implementation does not introduce speed and torque feedback and instead simply relies on the data from the flight accelerometer and distance sensors to achieve quadrotor altitude and attitude stability. Their model, furthermore, focuses on the entire quadrotor body, and no model for each individual motor was derived.

Their results showed a maximum steady-state error of 5° and a maximum system overshoot of 16% indicating the effectiveness of quadrotor flight stabilization using a PID controller (Li & Li, 2011).

Another study, by Bresciani (2008), focuses on the use of the PID technique for the attitude control algorithm of the quadrotor platform. He used the MATLAB Simulink tool to simulate the control system behavior to determine the performance of the system. The PID-based control system is running on an STR730 microcontroller.

For velocity and orientation data acquisition, the study highlights the use of an inertial measurement unit (IMU). The data acquired by the IMU are used for controlling the quadrotor's attitude stability. The IMU calculates the pitch, roll, and yaw movements of the quadrotor by utilizing three-axis accelerometers, three-axis magnetometers, and three-axis gyroscopes. Finally, with the use of a sonar device, the quadrotor implementation is able to perform a form of servo control for flight navigation.

The results show a maximum of 1° steady-state error for the pitch and roll and a maximum of 10° error for the yaw as obtained from the flight experimentations (Bresciani, 2008).

The study conducted by Oner et al. (2008) concentrates on introducing a new aspect of quadrotor control, a tilt-wing mechanism in which the propellers can be positioned vertically or horizontally depending on the flight mode that is intended to be achieved. The quadrotor platform is set up with four rotors and four wings wherein each rotor is mounted on a corresponding wing such that when the wings are tilted, the rotors tilt along with them.

The mathematical model of the quadrotor with the wing-tilt mechanism is then used to design the compensator for controlling the movement of the quadrotor in terms of the pitch, roll, and yaw, using a linear quadratic regulator (LQR) algorithm. The performance of the control system is then evaluated using the MATLAB Simulink tool from which the stability of movement of the quadrotor can be seen and verified (Oner et al., 2008)

The control structure presented in Anand, Hithesan, and Spreekumar's (2011) study exhibits the use of the attitude loop as the innermost control loop, which directly determines the PWM input commands and in effect directly drives the thrust generated by the motors and propellers.

2. QUADROTOR SYSTEM

An illustration of the top-level system integration of the whole quadrotor system is shown in Figure 3. This depicts the system flow of the various quadrotor states (e.g., rotor speed and current, attitude and altitude) to and from the dsPIC MCU for data logging and correct motor actuation. All control structures, i.e., speed-torque and altitude and attitude control, are implemented in discrete form. In order to determine the optimal controller for the quadrotor platform, the model for the brushless DC motor must be established.

2.1. Brushless DC Motor Model

The BLDC motor model used is based on the work of Stefan Baldursson (2005) on DC and BLDC motor modeling. The Simulink model of the BLDC motor, which is the DJI 2212 wye-

connected three-phase BLDC motor, is derived from the electrical and mechanical equations of a three-phase BLDC motor that the paper presents. An inverter model that is responsible for converting the DC voltage from the battery to the three-phase voltages that enable the motor to run is also adapted in order to model the ESC of the quadrotor. The BLDC and the ESC blocks together form the plant of the Simulink model.

The complete BLDC Simulink top-level model is shown in Figure 4. Also, the control loops, namely, (1) torque control, (2) speed control, (3) attitude control, and (4) altitude control are also incorporated in the Simulink model. The simulation results will then be verified through the constructed quadrotor platform.

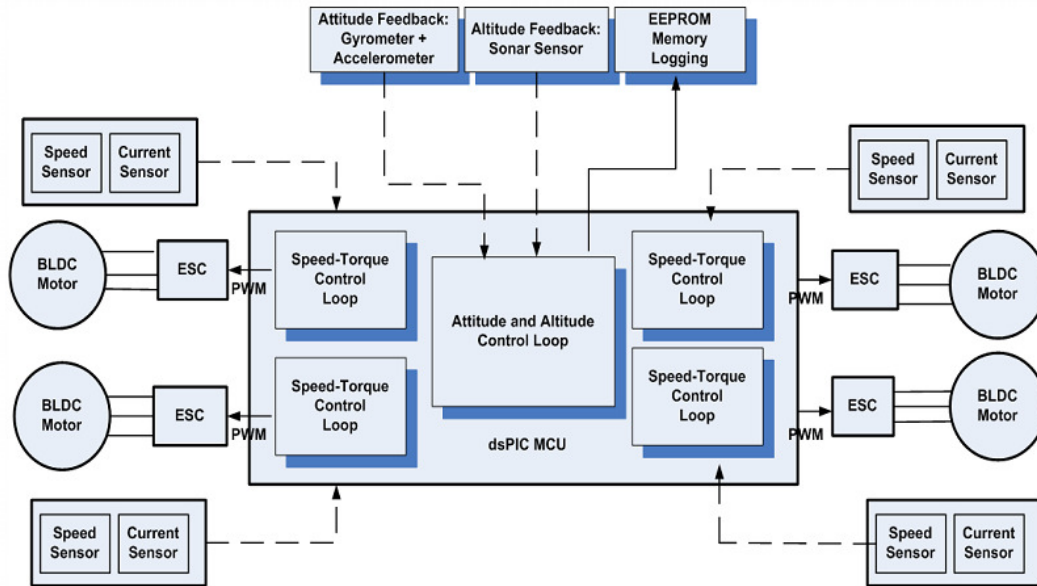


Figure 3. Top-Level System Integration of the Quadrotor Platform

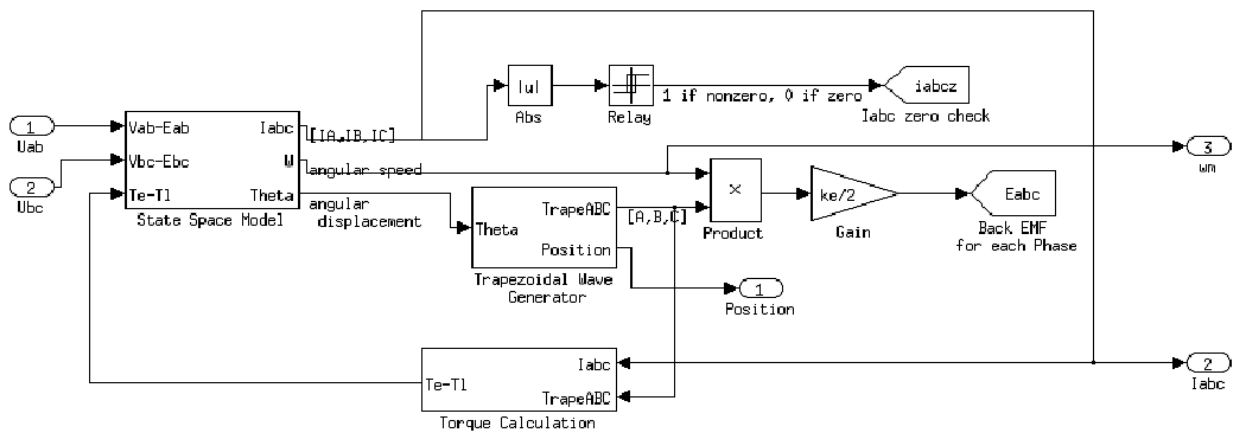


Figure 4. Brushless DC Motor Simulink Top-Level Model

The BLDC model can be represented by Figure 5. Each phase of the motor can be thought of as a conducting wire that is wound around parts of the stator. Each of these phase coils can then be

considered as a series combination of the phase resistance, the phase inductance, and what is called the phase back EMF. Put simply, the back EMF is the voltage generated across the coil due to the

rotation of the rotor magnets about that particular phase coil. Note that in this model, it is assumed that the values of the phase resistances R and phase inductances L are also the same.

The simplified electrical equations shown in Equation 2 of the BLDC are

$$\begin{aligned} V_{ab} &= R(i_a - i_b) + L \frac{d}{dt}(i_a - i_b) + e_a - e_b \\ V_{bc} &= R(i_a + 2i_b) + L \frac{d}{dt}(i_a + 2i_b) + e_b - e_c \end{aligned} \quad (2)$$

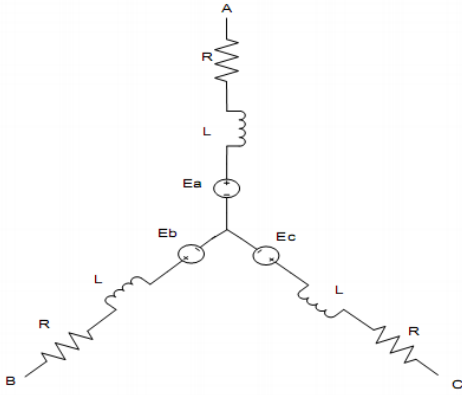


Figure 5. BLDC Motor Schematic Diagram

The mechanical equation of a BLDC motor is similar to the mechanical equations that govern a general DC motor, which come in the form of a summation of torques. This is given below in Equation 3:

$$T_E = k_f w_m + J \frac{dw_m}{dt} + T_L \quad (3)$$

where T_E is the electrical torque, k_f is the coefficient of friction, w_m is the rotor angular speed, J is the rotor inertia, and T_L is the load torque.

These electromechanical equations, Equations 2–3, comprise the “State Space Model” subsystem found in Figure 4.

The back EMF that each phase of the BLDC motor generates comes in a trapezoidal waveform due to the physical arrangements of the magnets and coils within the motor, with each phase back EMF being 120° out of phase from each other. To

account for this in the Simulink model, a simple solution is to utilize a look-up table consisting of the amplitudes of the trapezoidal wave, which is indexed by the electrical position of the motor. The electrical position is calculated from the mechanical position by multiplying it by half the number of poles of the motor. In a similar manner, a position integer ranging from 0 to 5 (0 being 0° – 59° , 1 being 60° – 120° , and so on) is also generated from the electrical angle for use by the inverter block later on.

The torque calculation is also placed under one subsystem. Note that the function $F(\theta)$ in Equation 4

$$T_E = \frac{K_t}{2} \left[F(\theta_e) i_a + F\left(\theta_e - \frac{2\pi}{3}\right) i_b + F\left(\theta_e - \frac{4\pi}{3}\right) i_c \right] \quad (4)$$

corresponds to the trapezoidal wave generated by the look-up tables. The difference between the electrical torque and the load torque is the value that is directly fed to the state space subsystem as can be seen in the figure of the overall model of the BLDC motor in Figure 4.

One last important thing to note in this model is that a go-to block is used in order to reference two vectors: (1) a vector corresponding to whether the phase currents are zero and (2) another one for the phase back EMF. These two go-to blocks are used in the inverter model.

The model of the inverter is implemented using an m -function that calculates the phase voltages to be outputted to the BLDC plant depending on the position of the rotor of the BLDC motor, the phase back-EMF values, and whether the current through each phase is zero. It determines the sequence of phase voltages that must be supplied to the motor for each 60° interval, in this case the values $V_{ab} - E_{ab}$ and $V_{bc} - E_{bc}$. The basis for the inverter m -function is taken from the table provided by Baldursson (2005) for determining the inverter output voltages as shown in Table 1.

In order to allow for PWM control, the inverter subblock is designed such that it is able to chop the phase operation of the motor, turning on and off

any phase within any 60° interval, allowing for the control of the average power that is delivered to each phase.

Table 1. Inverter Output Voltages Taken From BLDC Motor Modeling and Control (2005)

El. Angle	Diode Current	$v_{ab} - e_{ab}$	$v_{bc} - e_{bc}$
0° – 60°	$i_c \neq 0$ $i_c = 0$	$V_s - e_a + e_b$ $V_s - e_a + e_b$	$-e_b + e_c$ $\frac{1}{2}(-V_s + e_a - e_b)$
60° – 120°	$i_b \neq 0$ $i_b = 0$	$-e_a + e_b$ $\frac{1}{2}(V_s - e_a + e_c)$	$V_s - e_b + e_c$ $\frac{1}{2}(V_s - e_a + e_c)$
120° – 180°	$i_a \neq 0$ $i_a = 0$	$-V_s - e_a + e_b$ $\frac{1}{2}(-V_s + e_b - e_c)$	$V_s - e_b + e_c$ $V_s - e_b + e_c$
180° – 240°	$i_c \neq 0$ $i_c = 0$	$-V_s - e_a + e_b$ $-e_a + e_b$	$-e_b + e_c$ $\frac{1}{2}(V_s + e_a - e_b)$
240° – 300°	$i_b \neq 0$ $i_b = 0$	$-e_a + e_b$ $\frac{1}{2}(-V_s - e_a + e_c)$	$-V_s - e_b + e_c$ $\frac{1}{2}(-V_s - e_a + e_c)$
300° – 360°	$i_a \neq 0$ $i_a = 0$	$V_s - e_a + e_b$ $\frac{1}{2}(V_s + e_b - e_c)$	$-V_s - e_b + e_c$ $-V_s - e_b + e_c$

2.2. Brushless DC Motor Compensation

Figure 6 depicts the Simulink model of a compensated brushless DC motor. The chosen rise time for the current controller is 0.1 ms, whereas the rise time for the speed controller is chosen to be 1 ms. The speed controller has a zero at -0.012, whereas the current controller has a zero at -102.96. These would translate to controller gains shown in the Table 2 and employed in the “Speed Controller” and “Current Controller” blocks in Figure 6.

Table 2. Controller Gains of the BLDC Motor

PI Current Controller		PI Speed Controller	
k_p	k_i	k_p	k_i
1.69×10^2	1.74×10^{-4}	1.63	1.98×10^{-2}

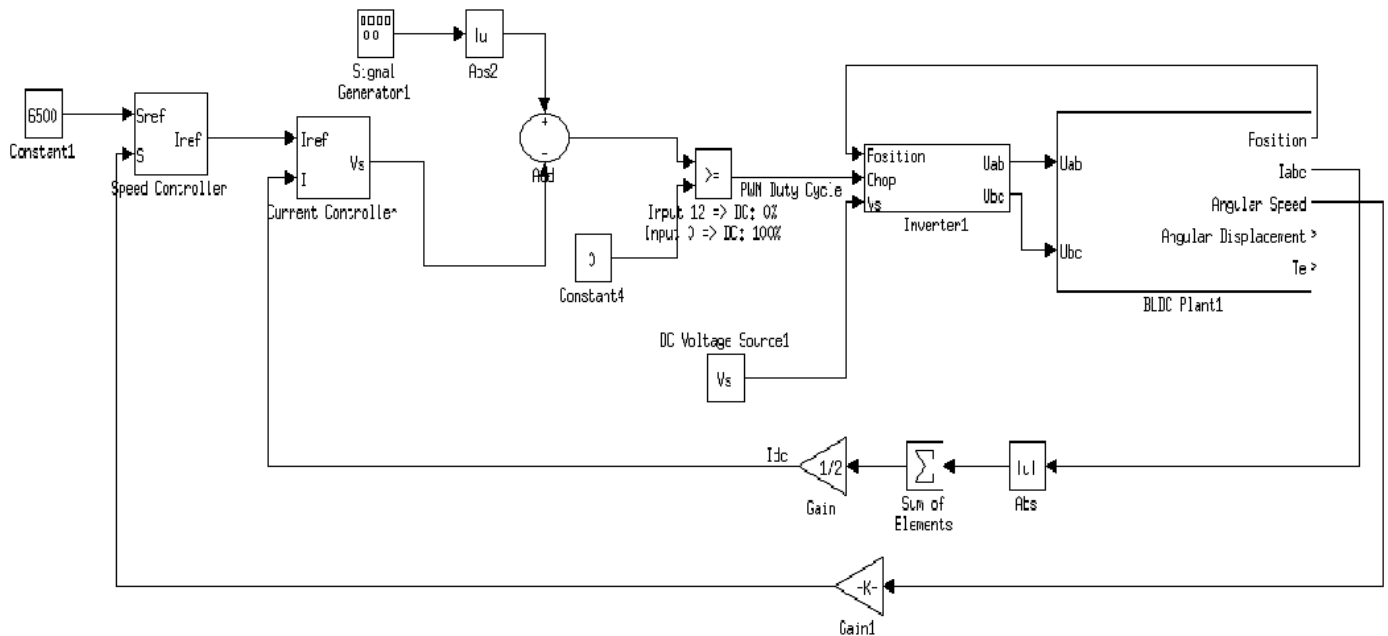


Figure 6. Speed-Torque Loop Control of a Brushless DC Motor

2.3. Attitude and Altitude Controllers

The control mixer in this study is applicable for a “+” mode quadrotor wherein the pitch axis lies along one of the arms of the quadrotor and the roll axis on the arm perpendicular to it. This is in

contrary to the “x” mode, where the pitch and roll axes lie along the lines between two arms.

After compensating the brushless DC motors, the whole quadrotor system simulation model is developed in Simulink. Figure 7 shows the

complete Simulink model of the quadrotor under study.

The attitude controller is tuned by initially setting the k_p and k_d constants to 0. The proportional constant is then slowly incremented until small oscillations in the form of strong tendencies to overshoot the reference attitude become observable. At this point, the k_p constant is decremented by small steps until the oscillations die out. The derivative constant is then increased with increments much lower than that for the proportional constant earlier. By carefully weighing the trade-offs that both constants introduce to the system and considering all nonidealities introduced by the actual model from the theoretical Simulink model, the specific values for the k_p and k_d constants are shown in Table 3.

In tuning the controller gains for the altitude loop, the same steps on how the attitude controller gains were derived were also followed. The controller constants for the altitude controller are given in Table 4 below.

Table 3. Attitude Controller Gains

Pitch		Roll		Yaw	
k_p	k_d	k_p	k_d	k_p	k_d
1.3	0.52	1.25	0.5	0.8	0.3

Table 4. Altitude Controller Gains

k_p	k_d
0.9	0.5

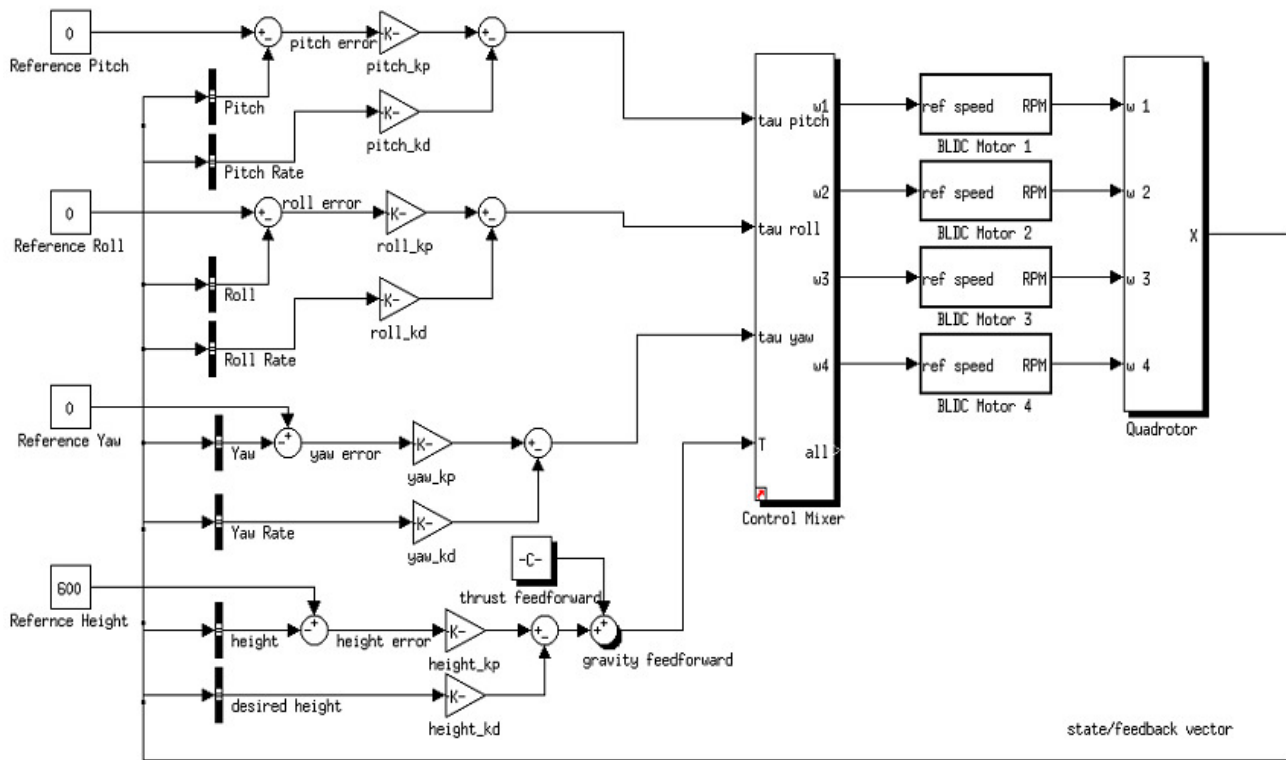


Figure 7. Simulink Quadrotor Model

3. RESULTS AND ANALYSIS

The quadrotor experimental platform is presented in Figure 8. It is named ARCHERS 3.0. Its name is derived from the university’s moniker

while the number represents its build version. Majority of its components including sensors and mechanical, electrical, and electronic components were bought commercially off the shelf in hobby stores located within Metro Manila.

The physical dimensions of the quadrotor ARCHERS 3.0 are given in Table 5.

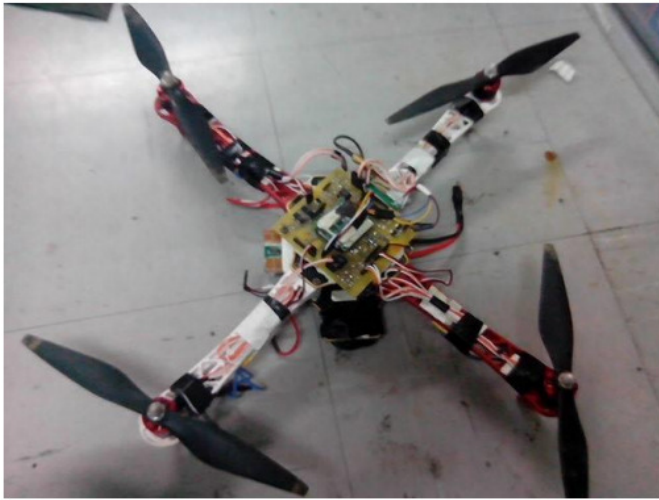


Figure 8. ARCHERS 3.0 Quadrotor Experimental Platform

Table 5. Quadrotor Physical Dimensions

Length (propeller to propeller)	71.12 cm
Length (motor to motor)	48.26 cm
Mass (without battery)	740 g
Mass (with battery)	920 g
Endurance	5 min

One unique attribute of this platform is that it has an optical tachometer extending from the middle to each of the four motors. This provides the necessary data for the speed control loop present in the control structure.

The BLDC motor parameters are shown in Table 6. Some quantities in Table 6 were experimentally determined while others were estimated and later verified in simulations and experiments.

Figure 9 shows the BLDC motor’s various response to varying desired angular speed and torque load. The BLDC motor is subjected to a dynamic loading torque conditions given by Equation 4:

$$Torque_{LOAD} = \begin{cases} 80mNm & 0 < t \leq 0.5 \text{ sec} \\ 0mNm & 0.5 < t \leq 1 \text{ sec} \\ 100mNm & 1 < t \leq 1.5 \text{ sec} \\ 0mNm & 1.5 < t \leq 2 \text{ sec} \end{cases} \quad (4)$$

Table 6. DJI 2212 Motor Parameters Summary

Nominal Voltage	12 V
No Load Speed	10,926 rpm
No Load Current	600 mA
Speed Constant	910 rpm/V
Back-EMF Constant	0.0011 rpm/V
Torque Constant	18.16 mNm/A
Phase Resistance	0.25 Ω
Phase Inductance	0.425mH
Rotor Inertia	0.00996 mkg·m ²
Number of Poles	14

Note that the desired speeds of 6,000–7,000 rpm were scaled by 40 so that the effects in the motor speed are seen when there is a sudden change in the torque being applied to the motor.

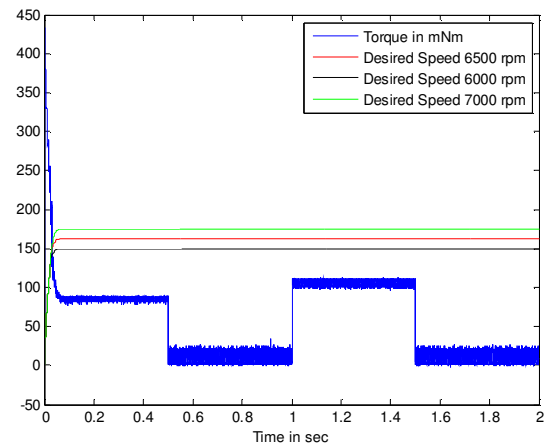


Figure 9. Simulated Speed and Torque Responses

It is evident in the transient response of the motor speed that there are no overshoots or undershoots but it quickly rises to the desired speed. Such effects are because of the proper tuning of the PID gains in the current and voltage controllers of the system. Another observation is that no matter what the load torque is, the motor is able to maintain the desired angular speed. For a

noncompensated system, the angular speed of the motor tends to decrease.

Figure 11 depicts an actual measurement from the platform during flight. Also note that at this point, the battery is fully charged.

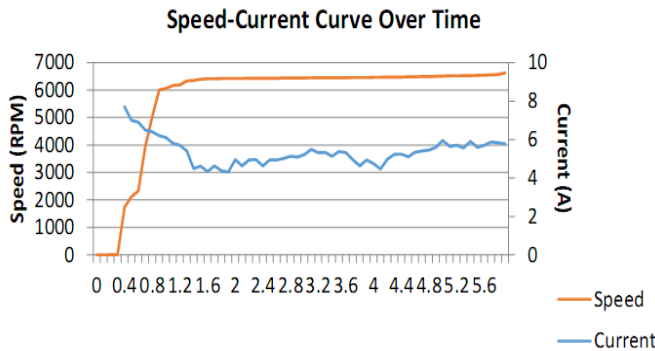


Figure 11. Speed and Torque Responses During Actual Flight

At times when the quadrotor is at flight, the power supply tends to drift in its nominal voltage. Shown in Figure 12 is the response of the system for such a scenario. Notice that the PID controller provides the appropriate duty cycle in order to keep the angular speed constant.

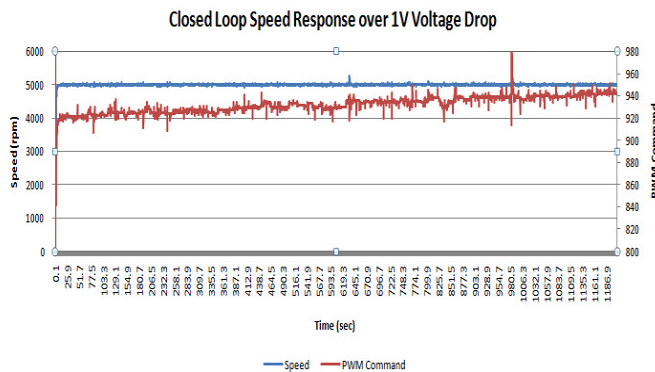


Figure 12. Speed and PWM Command Plot Over a 1-V Voltage Drop

The data in Figure 13 are taken with the quadrotor held in the roll axis while it is allowed to move freely in the pitch axis. Two motors with propellers are allowed to run to a speed sufficient for the attitude control to work, during which the angular data from the accelerometer, the gyrometer, and the complementary filter were obtained for observation.

As can be observed, the angle measurements derived from the accelerometer output becomes significantly noisy once the motor started spinning at time = 4.1 s because of the mechanical vibrations that the high-speed BLDC motor generates. The angle estimate from the accelerometer can be seen to fluctuate around the true angle with a standard deviation of 7.39°.

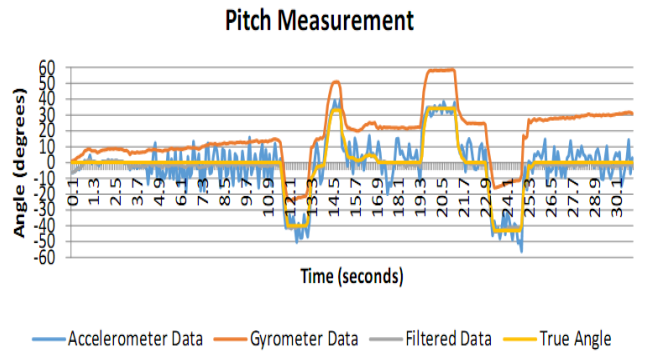


Figure 13. Attitude Data Comparison

On the other hand, the data obtained by numerically integrating the output of the gyrometer result in angle measurements that suffer much less from the mechanical noise generated by the motors. The readings, however, can be clearly seen to be drifting over time with the measurement having drifted from 0° to around 10° within the first 10 s of the test, during which the pitch axis is actually simply being held at 0°. In this regard, the output of the complementary filter can be seen to be significantly better than that from the individual sensors. Simply put, the measurement taken from the complementary filter takes the general form of the gyrometer data but with the accelerometer data used as a bias to correct the drift.

Height feedback is attained by using an ultrasonic sensor whose function involves sending an ultrasonic pulse and providing an output signal that is proportional to how long it takes for the signal to echo back for the host microcontroller, from which the height can be calculated. Table 7 shows the height measurements derived from the ultrasonic sensor, where it can be seen that the maximum percentage difference is less than 5%.

Table 7. Altitude Data Comparison

Actual Measurement (cm)	Sonar Data (cm)	Percentage Difference
4.8	5.09	1.47
9.6	9.65	0.13
25.6	24.81	0.78
42.4	50.58	4.40
74.4	77.72	1.09
99.5	104.14	1.14
149.2	152.4	0.53
202.1	205.74	0.45
252.1	240.24	1.20
303.3	292.64	0.89

Figure 13 (viewed per row, top to bottom, left to right) shows ARCHERS 3.0 in one of its test flights from take-off to landing, implementing the algorithm discussed above. It was held in the university grounds. ARCHERS 3.0 was controlled by a user through a wireless remote controller. In

another test flight, ARCHERS 3.0 achieved a maximum height of around 8 m.

The first three snapshots show ARCHERS 3.0 from its stationary position to take-off. At this point, the quad is almost 0.3 m from the ground.

The next set of three snapshots depicts ARCHERS 3.0 as it rises from 0.3 m to approximately 1.5 m.

The third set of three snapshots is when ARCHERS 3.0 rises from 1.5 m to its highest altitude (for this test flight) of around 5 m.

The fourth set of three snapshots shows ARCHERS 3.0 on its descent mode, while the last set of three snapshots depicts ARCHERS 3.0 on its final landing phase.

A noteworthy observation during this test flight was the presence of wind. The quadrotor was intentionally meant to fly in a controlled and indoor environment, and wind was never included in the model of the quad. However, this successful test flight has proven the robustness of the proposed and implemented control technique.





Figure 13.ARCHERS 3.0 Take-off to Landing

4. CONCLUSION

It has been shown through simulation and actual experiments that the proposed implementation of a speed and torque control of brushless DC motors to attain altitude and attitude control of a quadrotor can be achieved.

In this work, a working quadrotor system has taken flight based on component modeling instead of system modeling or considering the physics of the quadrotor platform, i.e., if we correctly control the motor speed and torque, the quadrotor will achieve its desired altitude while maintaining the correct attitude.

The speed and current control structure implemented within the usual attitude and altitude control allows the outer loops to be able to perform normally even if the motors and ESCs are not well matched. The inner loops manage any motor mismatch issue by automatically adjusting the command duty cycle if the desired set point is not achieved, allowing the outer loops, which run at slower frequencies, to work as intended.

Furthermore, this control structure allows the more important attitude control to work at the range of operation it was tuned at. This is because for typical attitude control loops that directly output the PWM command duty cycle, any drop in voltage would result in variations of performance of the attitude control.

With the addition of the inner control loops, the outer attitude loop performance remains the same even if the supply voltage drops over time. For as long as the battery is able to produce enough power to supply the demand of the motor, the inner loops will be able to adapt to any change in motor performance.

The stability of the quadrotor is verified by observing that the controller is able to hold the attitude in terms of the roll, yaw, and pitch angles of the quadrotor over a time duration of 10 min with a standard deviation of less than 5° and the altitude with a standard deviation of less than 50 cm. In one of its test flights, the quadrotor can achieve the required minimum height of 6 m and get there within less than 5 s.

REFERENCES

- Baldursson, S. (2005). *BLDC motor modelling and control*. Gothenburg, Sweden: University of Chalmers.
- Bresciani, T. (2008). *Modelling, identification and control of a quadrotor helicopter*. Lund, Sweden: Lund University.
- Corke, P. (2011). *Robotics, vision and control fundamental algorithms in MATLAB®*. Berlin: Springer.
- Hoffman, G., Huang, H., Waslander, S., & Tomlin, C. (2007). Quadrotor helicopter flight dynamics and control: Theory and experiment. In *Proceedings of the AIAA Guidance, Navigation and Control Conference* (pp. 1–20). Hilton Head, South Carolina: American Institute of Aeronautics and Astronautics.
- Li, J., & Li, Y. (2011). Dynamic analysis and PID control for a quadrotor. In *Proceedings of the 2011 International Conference on Mechatronics and Automation (ICMA)* (pp. 573–578). Beijing: IEEE.
- Oner, K.T., Cetinsoy, E., Unel, M., Aksit, M. F., Kandemir, I., & Gulez, K., (2008). Dynamic model and control of a new quadrotor unmanned aerial vehicle with tilt wing mechanism. *International Journal of Mechanical, Industrial Science and Engineering*, Vol. 2 No.9, pp. 12–17.
- Spreekumar, A., Hithesan, P., & Anand, M. K. (2011). *Design and implementation of the closed loop control of a quadrotor UAV for stability*. Coimbatore, India: Amrita School of Engineering.
- Weng, K. W., & Abidin, M. S. (2006). Design and control of a quad-rotor flying robot for aerial surveillance. In *Proceedings of the 2006 4th Student Conference on Research and Development* (pp. 173–177). Malaysia: IEEE.